American Mineralogist, Volume 81, pages 475–484, 1996

Reinvestigation of the annite = sanidine + magnetite + H_2 reaction using the f_{H_2}-sensor technique

GARY L. CYGAN,[1] I-MING CHOU,[1] AND DAVID M. SHERMAN[2]

[1]U.S. Geological Survey, 959 National Center, Reston, Virginia 22092, U.S.A.
[2]Department of Geology, University of Bristol, Bristol BS8 1RJ, U.K.

ABSTRACT

The decomposition of the iron mica, annite, to sanidine plus magnetite and vapor, $KFe_3AlSi_3O_{10}(OH)_2 = KAlSi_3O_8 + Fe_3O_4 + H_2$, has been reexamined experimentally with the use of a variety of buffers coupled with f_{H_2} sensors at 2 kbar and between 400 and 840 °C. Various capsule configurations were used in this study to delineate the equilibrium constant for this reaction in conjunction with ^{57}Fe Mössbauer spectroscopy measurements to monitor the oxy-annite component in mica in selected experiments. Results at the most reducing and highest temperature conditions of this study extend the annite stability field to higher temperature and f_{O_2} values than those defined in previous work. Lower temperature results indicate that the annite-sanidine-magnetite stability boundary does not intersect the hematite + magnetite + H_2O buffer at 400 °C as previously reported but rather is subparallel to the buffer curve at lower f_{O_2} values. The equilibrium f_{H_2} (in bars) for the assemblage annite + sanidine + magnetite + vapor at 2 kbar and between 400 and 840 °C can be described by the relation $\log f_{H_2}\ (\pm 0.08) = 13.644 - (17368/T) + (5.168 \times 10^6)/T^2$, where T is temperature in kelvins.

INTRODUCTION

The decomposition reaction of annite, the iron biotite, to sanidine plus magnetite (ASM)

$$KFe_3AlSi_3O_{10}(OH)_2 = KAlSi_3O_8 + Fe_3O_4 + H_2 \quad (1)$$

has been the topic of numerous studies involving a variety of experimental techniques. Calculations based on this reaction are used to infer redox conditions during magmatic crystallization and subsequent alteration (Wones 1981). Of particular interest from an experimental point of view is the large f_{H_2} range at geologically interesting temperatures, approximately 0.01 to >500 bars (at a total pressure of 2 kbar). If we assume that sanidine and magnetite are pure phases, the equilibrium constant can be defined as

$$K_1 = \frac{f_{H_2}}{a_{annite}} \quad (2)$$

where a_{annite} is the activity of the annite component, $KFe_3AlSi_3O_{10}(OH)_2$, in mica. On the basis of new measurements made with improved experimental techniques, this study revises the shift of the reported equilibrium f_{H_2} values of previous studies. We also use current buffer calibrations to demonstrate the inconsistencies and shortcomings of the previous experimental methods. We specifically focus on the questionable assumption that the redox states of a buffering system may be calculated accurately from equilibrium thermochemical data. Finally, we use f_{H_2}-sensor techniques (Chou 1987a; Chou and Cygan 1990) to add new information on Reaction 1 over a wider temperature range (400–840 °C) at 2 kbar. The equilibrium redox conditions for Reaction 1 occur at highly reducing and highly oxidizing environments at high and low temperature, respectively.

PREVIOUS INVESTIGATIONS

The log K of Reaction 1, assuming pure solid phases, may be depicted conveniently on a log f_{H_2} vs. $1/T$ diagram. Pertinent data points from previous investigations are presented in Figure 1, modified from Chou and Cygan (1990). Eugster (1957, 1959) and Eugster and Wones (1962) were the first to use solid O_2 buffers to impose defined f_{O_2} values in hydrothermal experimentation. They used thermochemical data to calculate the equilibrium f_{H_2} values for specific buffers at a given P and T, and reaction direction was determined by X-ray and optical examination of experimental products. Their results for Reaction 1 can be described by Equation 3, which is shown in Figure 1 as the solid line labeled as ASM (E and W 1962):

$$\log f_{H_2} = -9215/T + 10.99 \quad (3)$$

where T is in kelvins. Other past investigations shown in Figure 1 used a variety of redox buffers and techniques. We refer the reader to the discussion in Chou and Cygan (1990), which provides details of experimental hydrothermal techniques and an assessment of the discrepancies among studies.

The technique of in situ measurement of f_{H_2} was developed by Chou and Eugster (1976) using the Ag + AgCl + HCl assemblage as a sensor. Calibrations of several buffers (Chou 1978) demonstrate the sensor's utility and

0003–004X/96/0304–0475$05.00

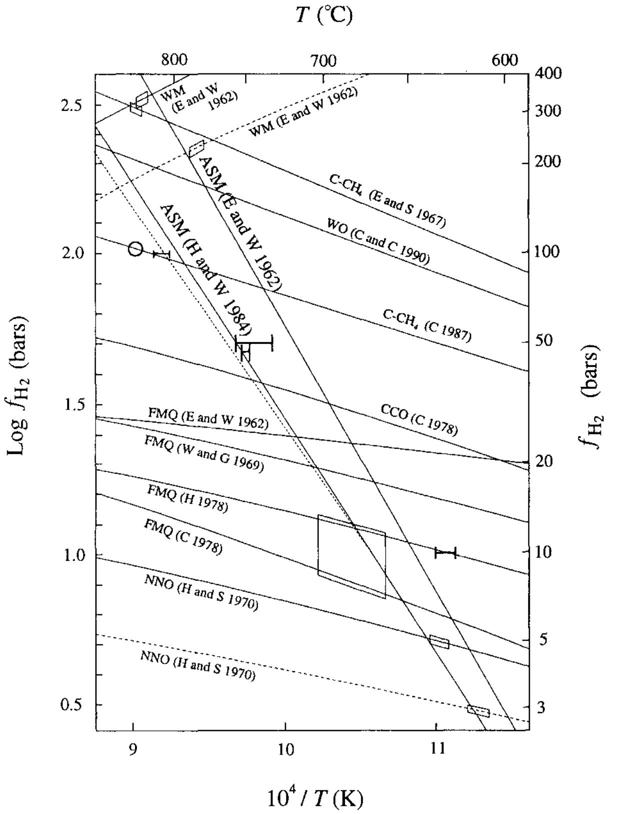

FIGURE 1. Log f_{H_2} vs. $10^4/T$ (K) diagram modified from Chou and Cygan (1990, their Fig. 7) showing results of previous investigations of Reaction 1. The dashed and light solid lines depict various buffering assemblages at 1 and 2 kbar, respectively: NNO (Ni + NiO + H_2O) from Huebner and Sato (1970; H and S); FMQ (Fe_2SiO_4 + Fe_3O_4 + SiO_2 + H_2O) from Chou (1978; C), Hewitt (1978; H), Wones and Gilbert (1969; W and G), and Eugster and Wones (1962; E and W); CCO (Co + CoO + H_2O) from Chou (1978); WO (WO_2 + H_2O) steady-state assemblages from Cygan and Chou (1990; C and C); WM ($Fe_{1-x}O$ + Fe_3O_4 + H_2O) from Eugster and Wones (1962); and the assemblage (C + CH_4) from Chou (1987b; C) and Eugster and Skippen (1967; E and S). The steeply dipping heavy solid lines show the position of Equation 1 determined by Eugster and Wones (1962) and, subsequently, by Hewitt and Wones (1984; H and W). The heavy dotted line is based on the data of Cygan et al. (1991). Parallelograms indicate the various reversal points, including uncertainties in the calibrations. These data are from Eugster and Wones (1962) along the FMQ buffer curve at 2 kbar and the NNO and WM buffer curves at 1 and 2 kbar, and from Rutherford (1969) along the C-CH_4 and FMQ buffer curves at 2 kbar. The NNO curves were recalculated using data from Huebner and Sato (1970). The horizontal bars are data gathered by Wones et al. (1971) using the Shaw membrane technique at 10, 50, and 100 bars f_{H_2}, and by Hewitt and Wones (1981) from the datum at 47 bars f_{H_2}. See text for additional explanation.

show that f_{H_2} values for buffers calculated on the basis of thermochemical data may lead to spurious results (Chou 1987a, 1987b; Ziegenbein and Johannes 1980; Cygan and Chou 1990; Cygan et al. 1991). For example, calibrated f_{H_2} values for the C + CH_4 buffer are ~0.3–0.6 log units lower than the calculated values at 2 kbar and between 650 and 800 °C (see Fig. 1 and Chou 1987b). Therefore, we conclude that the reversal point for Reaction 1 on the C + CH_4 buffer given by Rutherford (1969) should be shifted to a lower f_{H_2} value such as the one indicated by the open circle in Figure 1. This conclusion is sound given that equilibrium redox control in these experiments has never been reached. This can be attributed to H_2 diffusion through gold membranes and leakage to or from the pressure medium in certain hydrothermal configurations (Chou and Cygan 1990), as well as the sluggishness of certain buffer reactions such as C + CH_4 (Chou 1987b) and FMQ (Chou 1978; Chou and Cygan 1990). We use the term "leakage" to indicate the measurable gain or loss of H_2 in the gold capsule resulting from the necessary diffusion through the gold-capsule wall coupled with relatively rapid adsorption and desorption processes at the pressure medium–capsule-membrane interfaces; the term is not used to indicate faulty welds on the capsule. Therefore, H_2 leakage not only affects equilibrium determinations at extremely reducing conditions but also at very oxidizing conditions such as the MnO + Mn_3O_4 + H_2O (MNO) or MH buffers. In highly reduced assemblages, H_2 may leak out of the gold outer walls of the capsule, whereas in very oxidized experiments H_2 may leak into the gold capsule. In the latter case, sluggish permeation of H_2 through the inner platinum capsules, H_2 leakage from the pressure medium into the gold container, or some combination of the two (Chou and Cygan 1990) can result in higher f_{H_2} values than presumed. We conclude that most results of previous experiments conducted at both extremely reducing and extremely oxidizing conditions are affected by H_2 leakage. On the other hand, we find that the results of studies conducted on or near the f_{H_2} conditions produced by the nickel + nickel oxide + H_2O buffer (NNO) under argon or H_2O external pressure medium are reasonably accurate because f_{H_2} differences between the buffer system and the pressure medium are usually small. In addition, calibrations indicate that NNO accurately buffers f_{H_2} values over a wide range of temperature conditions (Chou 1986; Chou and Cygan 1990). Therefore, an analysis of the ASM equilibrium would suggest that the data obtained along the NNO buffer are accurate.

EXPERIMENTAL TECHNIQUES AND PROCEDURES

Standard hydrothermal pressure vessels made of Stellite 25 (any use of trade, product, or firm names in this publication is for descriptive purposes only and does not imply endorsement by the U.S. Geological Survey), a Co-based alloy, with an 8 mm i.d. were used. Temperatures were monitored using calibrated chromel-alumel thermocouples with an accuracy of ±3 °C. Pressures were monitored by Heise gauges with an accuracy of ±30 bars for argon and H_2O pressure media. Experiments made with CH_4 pressure medium required periodic recharging because of H_2 leakage through the pressure-vessel wall, and at the highest temperature investigated the pressure uncertainty is ±50 bars.

Starting material

Annite was synthesized using a stoichiometric mix of $KAlSi_3O_8$ gel (made from nitrate solutions) and iron oxalate ($FeC_2O_4 \cdot 2H_2O$) by the reaction

$$\begin{aligned} &KAlSi_3O_8 + 3(FeC_2O_4 \cdot 2H_2O) + [(6 + x)/4]O_2 \\ &\quad = K(Fe^{2+}_{3-x}Fe^{3+}_{x})AlSi_3O_{10+x}(OH)_{2-x} \\ &\qquad + [(10 + x)/2]H_2O + 6CO_2 \qquad (4) \end{aligned}$$

where x represents the oxy-annite component in the mica and is established by the ambient f_{H_2} value during synthesis. The mix was sealed into gold capsules (9.1 mm o.d., 0.26 mm wall thickness, 38 mm long) and run in Ni-based Inconel hydrothermal pressure vessels at 2 kbar argon pressure and 500 °C for 5–7 d. A portion of this synthesized annite was then annealed at 2 kbar for 3–7 d at the f_{H_2} conditions defined by the NNO, Co + CoO + H_2O (CCO), and WO_2 + H_2O (WO) assemblages and at T = 555, 650, and 775 °C, respectively. The Fe^{3+}/Fe^{2+} ratios of these annealed samples of annite were characterized by ^{57}Fe Mössbauer spectroscopy, discussed below, and these samples were used as additional starting material. Sanidine was synthesized from a $KAlSi_3O_8$ gel at 550 °C and 1 kbar for one week. Magnetite was synthesized from a stoichiometric mix of iron metal and Fe_2O_3 plus a 1 M NH_4Cl solution at 250 °C and vapor-saturated pressure for 3 d in a large (30 cm^3), Teflon-lined Morey vessel. Powder X-ray patterns and optical examination indicate complete reaction of the initial components to the desired starting compositions.

Additional solid redox buffer materials were obtained commercially (Co, CoO, and WO_2) or synthesized (wüstite, MnO, and Mn_3O_4) using standard hydrothermal or gas-mixing procedures. To synthesize wüstite, reagent-grade hematite was fired to ~600 °C, then packed into a silver-palladium bucket and run for 4 h at 1040 °C in a vertical, one-atmosphere gas-mixing furnace using appropriate mixtures of CO_2 and H_2 to control the f_{O_2} at $\sim 10^{-14}$. The wüstite produced was black and nonmagnetic and gave all characteristic X-ray peaks of the mineral. MnO was prepared by heating MnO_2 at 800 °C in an appropriate reducing mix of Ar-H_2 atmosphere for 15 h. Mn_3O_4 was also prepared from MnO_2 but was heated at 1100 °C for 20 h in air.

Capsule configurations

Figure 2 shows the capsule arrangements used in this study. Experiments made at $T > 700$ °C and f_{H_2} values greater than those defined by CCO required high f_{H_2} conditions. These conditions were obtained using configuration A (Fig. 2A), in which the C + CH_4 buffer (Chou 1987b) is used and f_{H_2} at P and T is monitored by the f_{H_2} sensor of the type Ag + AgBr + HBr. The experimental charge was contained in a platinum tube (1.85 mm o.d., 1.54 mm i.d., 19 mm long) consisting of an assemblage of either annite + H_2O or sanidine + magnetite + H_2O. Further information on the use of the C + CH_4 buffer and precautions are given in Chou (1987b). The other configuration for high-temperature experiments (Fig. 2B) uses the CCO buffer under argon external pressure or the steady-state H_2 source, WO, in a traditional arrangement under CH_4 external pressure; information on the use of the latter assemblage is given in Cygan and Chou (1990). The H_2 environment in the capsule configurations we used has been demonstrated to be a steady-state system, which is principally dependent upon the f_{H_2} gradients of the capsule interior and exterior, as discussed earlier. Some experiments on the WO assemblage at $T > 800$ °C were made in H_2O pressure medium to take advantage of H_2 leakage from gold capsules in a quasi-predictable manner. The f_{H_2} values imposed by the WO buffer assemblage coupled with an H_2O pressure medium are lower than the calibrated values obtained under argon pressure. This allowed f_{H_2} conditions intermediate to those defined by the WO and CCH_4 assemblages. A

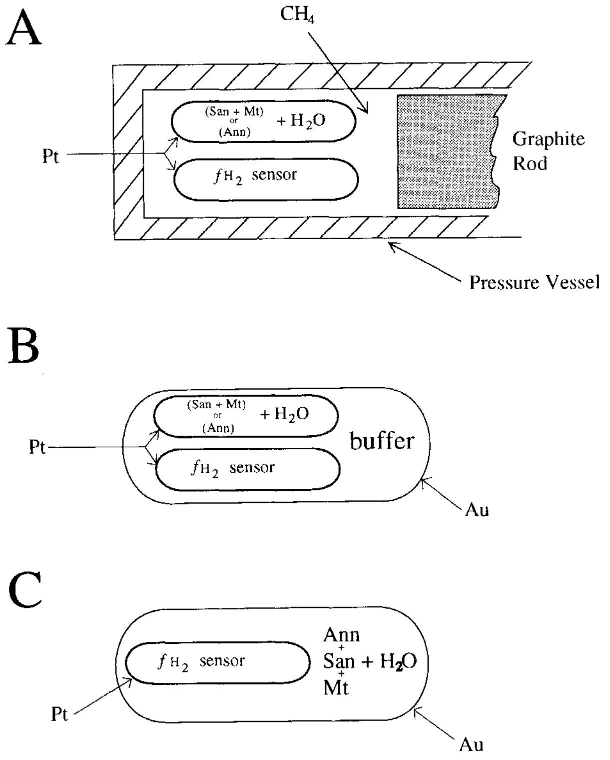

FIGURE 2. Capsule configurations used in this study. (**A**) CH_4 pressure medium and a graphite filler rod making up the buffer, plus an f_{H_2} sensor and the experimental charge in platinum capsules containing either annite (Ann) + H_2O or sanidine (San) + magnetite (Mt) + H_2O. (**B**) The traditional hydrothermal method of redox control using a double-tube technique with the addition of an f_{H_2} sensor. (**C**) The setup primarily used for the low-temperature experiments. Consists of the complete Ann + San + Mt + H_2O assemblage and an f_{H_2} sensor. The f_{H_2} sensor was constructed of very thin walled (0.1 mm) platinum.

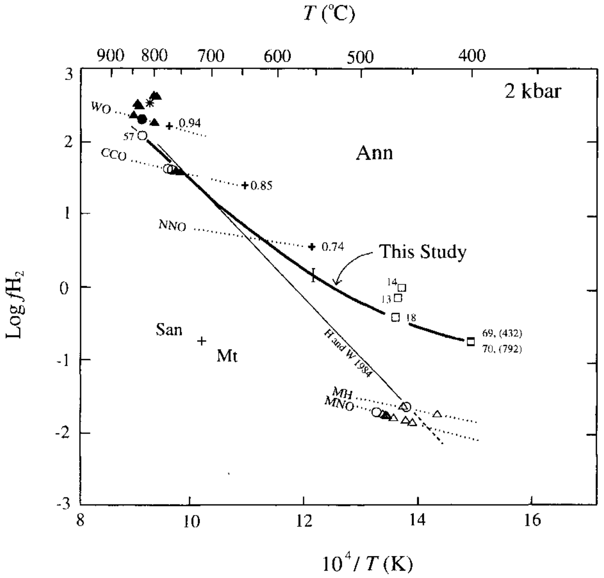

FIGURE 3. Log f_{H_2} vs. $10^4/T$ (K) plot showing selected experimental results at 2 kbar. Annite is stable above the curves, sanidine + magnetite, below. Results of this study are represented as a heavy solid line (Eq. 10). The light solid line is from Hewitt and Wones (1984). Dotted lines running oblique to experimental data curves denote calibrated buffering assemblage data. See text for sources. Symbol definitions for this study are as follows: solid triangles = San + Mt → Ann, solid circle = Ann → no reaction, open triangles = San + Mt → no reaction, open circles = Ann → San + Mt, and open squares = complete assemblage Ann + San + Mt. Data points lying off the dotted buffer curves at high T are results of experiments using the system-dependent C + CH_4 assemblage. Experiment numbers are given alongside; experiment duration is measured in hours, shown in parentheses. Uncertainties in log f_{H_2} are denoted by the vertical bar. Bold plus signs indicate where starting annite material is annealed, numbers alongside give X_{Fe} values determined by Mössbauer spectroscopy. The asterisk indicates the equilibrium point determined by Eugster and Wones (1962) for the reaction annite = fayalite + leucite + magnetite + vapor.

more complete description of the construction and use of f_{H_2} sensors is given in Cygan and Chou (1990). Uncertainties in f_{H_2} measurements are ±1%.

Capsule configurations B and C (Figs. 2B and 2C, respectively) were used for experiments at temperatures <470 °C and f_{H_2} conditions less than or equal to those defined by NNO. In Figure 2C, the equilibrium f_{H2} conditions determined by the ASM assemblage at P and T are recorded by the f_{H_2} sensor. Two experiments made at 400 °C did not contain sensors.

EXPERIMENTAL RESULTS

Three annite samples having different oxy-annite contents were obtained by annealing the initial synthetic annite at the T and f_{H_2} conditions shown by bold plus signs in Figure 3. Approximately 100 mg of each annealed annite sample was reserved for determination of X_{Fe}, the molar ratio of $Fe^{2+}/(Fe^{2+} + Fe^{3+})$, by Mössbauer spectroscopic analysis. Analyses were obtained by using a ^{57}Co source and a 512 channel analyzer on an Austin Scientific Associates spectrometer; counts per channel were always $> 10^6$. The spectra were fitted to four quadrupole doublets corresponding to Fe^{2+} and Fe^{3+} in the M1 and M2 octahedral sites. Attempts to include tetrahedral Fe^{3+} did not produce statistically significant improvements in the fits. The ratio of Fe in the M1 and M2 sites is very poorly determined by the fit to the Mössbauer spectra; large changes in the area ratio of Fe in the M1 and M2 sites results in only small changes in the goodness-of-fit parameter (either MISFIT or Chi^2). This is because of the large overlap of the M1 and M2 quadrupole doublets. However, the X_{Fe} value is very insensitive to the manner in which Fe is partitioned between the M1 and M2 sites in the spectrum fitting procedure. The uncertainty in the calculated X_{Fe} value is estimated to be ±0.05. Values of X_{Fe} obtained using the NNO buffer at 550 °C, CCO at 650 °C, and WO at 775 °C are 0.74, 0.85, and 0.94, respectively (bold plus signs in Fig. 3). The data show an increase in Fe^{2+} as the f_{H_2} of the annealing condition increases, similar to the observations made by Wones et al. (1971), Partin et al. (1983), and Rebbert and Hewitt (1986).

X-ray and optical microscopic examinations of the annealed annite samples indicate that no additional phases are present. Unit-cell refinements were determined with the use of the program of Appleman and Evans (1973). Qualitative assessment of the 001 reflection indicates a progressive increase of c unit-cell dimension with increasing f_{H_2}, consistent with the X-ray data of Wones and Eugster (1965) and the X-ray and Mössbauer determinations of Ferrow (1990). The c dimensions are 10.264(4), 10.286(6), and 10.295(10) Å for the initial annite samples synthesized in the intrinsic pressure-vessel f_{H_2} and annealed on the NNO and CCO assemblages, respectively.

Figure 3 displays pertinent buffer curves and our experimental results at 2 kbar. Experimental data are given in Table 1. Buffering assemblages are shown as dotted lines. Sources of individual buffer f_{O_2} values are collectively published in Chou (1987a), Haas (unpublished data) for MH and MNO, Huebner and Sato (1970) for NNO, and Chou (1987a) for CCO. These values are converted to log f_{H_2} by means of the relation

$$H_2 + 0.5O_2 = H_2O \qquad (5)$$

where the equilibrium constant, K_W, is defined as

$$K_W = f_{H_2O}/(f_{H_2})\cdot(f_{O_2})^{0.5}. \qquad (6)$$

Data for f_{H_2O} and K_W were taken from Burnham et al. (1969) and Robie et al. (1979), respectively. The C + CH_4 assemblage is not represented on the diagram because it is system dependent (Chou 1987b).

Chou (1987a) demonstrated that the measured chloride concentration in an f_{H_2} sensor is proportional to f_{H_2} at P, T, or

$$(f_{H_2})_{P,T} = K'(m_{HCl})^2_{P,T} \approx K'(M_{Cl^-})^2_{1\text{ bar, }25\,°C} \qquad (7)$$

TABLE 1. Experimental results at 2 kbar

Expt.	T (°C)	P medium	t (h)	Starting assemb.	Products and remarks	f_{H_2}-sensor data M_{Br^-} or M_{Cl^-}*	
						Initial	Final
				Experiments using configurations A and B			
WO							
21	841	CH_4	6	San + Mt	Ann + San + Mt	n.u.	
23	795	CH_4	7	San + Mt	Ann	3	0.5983
31	830	CH_4	5	Ann	Ann	H_2O	0.5834
32	830	CH_4	5	San + Mt	Ann	n.u.	
34	830	CH_4	6	San + Mt	Ann	n.u.	
C-CH_4							
40	800	CH_4	6	San + Mt	Ann + San + Mt	H_2O	0.5410
49	840	CH_4	5	San + Mt	Ann + (San + Mt)	1.5	0.4359
50	797	CH_4	8	San + Mt	Ann + (San + Mt)	1.5	0.3879
52	832	CH_4	7	San + Mt	Ann + (San + Mt)	1.5	0.4108
CCO							
1	710	Ar	72	San + Mt	exhausted buffer, Ann	n.u.	
2	800	Ar	24	San + Mt	questionable buffer, San + Mt	n.u.	
3	751	Ar	48	San + Mt	Ann + San + Mt	n.u.	
5	750	Ar	48	San + Mt	minor Ann	n.u.	
6	760	Ar	76	Ann	San + Mt	n.u.	
7	760	Ar	72	Ann	San + (Mt)	n.u.	
MNO							
44	475	Ar	30	San + Mt	San + Mt	n.u.	
45	461	Ar	28	San + Mt	San + Mt	n.u.	
46	445	Ar	27	San + Mt	San + Mt	n.u.	
37	470	Ar	30	San + Mt	San + Mt	n.u.	
8	471	Ar	336	San + Mt	San + Mt	n.u.	
9	450	Ar	672	San + Mt	San + Mt	n.u.	
10	480	Ar	408	Ann	Ann + San + Mt	n.u.	
MH							
41	450	Ar	29	An	Hm + San	n.u.	
42	425	Ar	29	San + Mt	San + (Hm + Mt)	n.u.	
43	453	Ar	28	San + Mt	San + Mt	n.u.	
				Experiments using the full assemblage			
11	456	Ar	220	Ann + San + Mt	Ann + San + Mt	H_2O	0.2207
13	459	Ar	264	NNO Ann** + San + Mt	Ann (X_{Fe} = 0.72) + San + Mt	H_2O	0.1922
14	458	Ar	264	CCO Ann** + San + Mt	Ann (X_{Fe} = 0.69) + San + Mt	H_2O	0.2283
38	470	Ar	720	Ann + San + Mt	San + Mt	H_2O	0.2450
69	400	Ar	432	Ann + San + Mt	Ann + San + Mt	H_2O†	0.2337
70	400	Ar	792	Ann + San + Mt	Ann + San + Mt	H_2O†	0.2149
				Modified experiments			
18‡	460	Ar		Ann + San + Mt	Ann + San + Mt	H_2O	0.1547
54	750	(CH_4/Ar)§	18	Ann	Ann	1.5	0.4471
56	820	H_2O	4	San + Mt on WO‖	Ann + (San + Mt)	1.5	0.3894
57	822	H_2O	6	Ann on WO‖	Ann + San + (Mt)	H_2O	0.2552

Note: Table shows the following: (1) Experiments using configurations A and B shown in Figure 2 with various pressure media. WO, C-CH_4, CCO, MNO, and MH indicate buffering assemblage. The f_{H_2} sensors were included for selected experiments on buffers more reducing than CCO. (2) Experiments using the full assemblage of annite + sanidine + magnetite + H_2O; see Figure 2C. (3) Experiments conducted with various modifications of experiments described in parts 1 and 2 above. Ann, San, Mt, and Hm indicate annite, sanidine, magnetite, and hematite, respectively. Annite was synthesized at an f_{H_2} condition slightly lower than NNO conditions. Abbreviation n.u. = not used in experiment. Parentheses indicate minor abundances.

* Initial concentrations used in sensors are in M_{Cl^-} except for experiments at $T \geq 750$ °C, where M_{Br^-} is used (M = molarity).

** NNO and CCO denote annite compositions annealed on these buffers, X_{Fe} = 0.74 and 0.85, respectively.

† The f_{H_2} sensors are constructed from thin walled (0.1 mm) platinum.

‡ Uses two gold capsules. Inner capsule is configured as in Figure 2C, outer capsule contains MH buffer to establish an H_2 sink for the inner capsule.

§ Pressure medium consists of a mixture of argon and CH_4 in the approximate initial pressure ratio 10:1.

‖ Pressure medium is H_2O. Capsule is configured as in Figure 2B with WO as buffer.

where K' is a constant and m and M are molality and molarity, respectively. Both Ag + AgCl + HCl and Ag + AgBr + HBr types of f_{H_2}-sensor systems are used in this study, and Equation 7 is analogous for HBr with appropriate constants [see Chou (1987a) for a complete discussion of f_{H_2} sensors]. Conversion of the measured $M_{Br^-\,(25\,°C,\,1\,bar)}$ values to log f_{H_2} is given in Table 2 for experiments performed under the C + CH_4 buffer. The error bar shown in Figure 3 represents the uncertainty in computing log f_{H_2}, including the uncertainty in f_{H_2}-sensor measurements.

Results of our experiments on the CCO buffer indicate a small displacement, within the uncertainty of our measurements, of Reaction 1 to lower log f_{H_2} conditions than those of Hewitt and Wones (1984). The experiments at the highest temperatures investigated, up to 840 °C, were

TABLE 2. Computation of log f_{H_2} and log f_{O_2} values from f_{H_2}-sensor data for experiments made on the C + CH_4 buffer at 2 kbar

Expt.	T (°C)	$(M_{Br^-})_{1,25}$	$-\log(M_{Br^-}^{CCO})$	$\log(f_{H_2})^{CCO}$	log $f_{H_2}^{S}$	log f_{H_2O}	log K_W	log f_{O_2}
40	800	0.267	0.801	1.671	2.74	3.198	9.171	−17.427
49	840	0.361	0.767	1.721	2.536	3.218	8.737	−16.109
50	797	0.411	0.793	1.695	2.459	3.195	9.186	−16.900
52	832	0.386	0.774	1.711	2.487	3.214	8.821	−16.188
57*	822	0.255	0.782	1.699	2.078	3.209	8.928	−15.594

Note: Measured Br^- molarity in the f_{H_2} sensor at 1 atm and 25 °C. CCO is used as the reference buffer. Values of $-\log(M_{Br^-}^{CCO})$ are computed from log $M_{Br^-} = -(1003.7/T\ K) + 0.134$ for the Co + CoO + H_2O buffer (Cygan and Chou 1990, their Eq. 6). Log $f_{H_2}^{CCO} = \log f_{H_2O} - \log K_W - \frac{1}{2}\log f_{O_2}$. Values of log f_{O_2} are from Chou (1987a); $f_{H_2}^{S} = f_{H_2}^{CCO}(M_{Br^-}^{S}/M_{Br^-}^{CCO})^2$, where superscripts S and CCO indicate sample and calibration values for CCO buffer, respectively. Values of log f_{H_2O} are from Burnham et al. (1969). Equilibrium constant, K_W, for the reaction $H_2 + \frac{1}{2}O_2 = H_2O$; data from Robie et al. (1979). Log $f_{O_2} = 2(\log f_{H_2O} - \log f_{H_2} - \log K_W)$.

* Exposed to the WO buffer assemblage with H_2O as the external pressure medium; see text for discussion.

conducted with the reducing assemblages WO and C + CH_4 in an attempt to intersect the reaction

$$3 \text{ annite} = 3 \text{ fayalite} + 3 \text{ leucite} + \text{magnetite} + 2\,H_2O + H_2. \quad (8)$$

Annite was reported to decompose at 825 ± 5 °C and log $f_{O_2} \approx -16.9$ (Eugster and Wones 1962; converted to f_{H_2} and shown as the asterisk in Fig. 3). Hewitt (personal communication) reported the location of Reaction 8 to be at a log f_{H_2} value of 1.85 ± 0.09 between ~820 and 835 °C. We find that annite is stable at temperatures up to 840 °C, as shown in Figure 3, and we acknowledge this discrepancy. To locate the equilibrium boundary of Reaction 8, alternative experimental techniques, such as use of the internally heated pressure vessel, with higher T and controlled f_{H_2} capabilities, are required (e.g., Scaillet et al. 1992).

In experiment 57, enhanced H_2 leakage was created by pairing a reducing buffer with H_2O rather than CH_4 as the external pressure medium. This experiment used configuration B, the WO assemblage, and an f_{H_2} sensor. H_2-sensor uncertainties are ±0.02 in log f_{H_2}. Discussion of a time-dependence study and equilibrium implications of f_{H_2}-sensor measurements is given in Chou (1987a). Note that the f_{H_2} value measured by the sensor in this experiment is displaced to lower f_{H_2} values than those of the calibrated WO curve (dotted line) using CH_4 as the external pressure medium. This experiment and experiment 21 at 841 °C represent a reversal of Reaction 1. The location of the annite + vapor field is therefore increased to higher temperature and lower f_{H_2} in comparison with the curve representing the data of Hewitt and Wones (1984) (see Fig. 3).

Low-temperature and less reducing experiments were made on the MH and MNO buffers by using capsule configuration B without an f_{H_2} sensor. These experiments all resulted in magnetite + sanidine, contrary to the predictions of Equation 3 (see Table 1 and Fig. 3). This may be due to inaccurate buffer control in previous experiments at low temperatures, below approximately 600 °C, and redox conditions more oxidizing than those associated with NNO (Chou and Cygan 1990). It is standard practice to use X-ray techniques to determine whether the buffer assemblage is present after an experiment; however, we found that this was necessary but insufficient to insure an operating buffer. The additional precaution of monitoring the ambient redox condition at P and T with f_{H_2} sensors yields the actual f_{H_2} value for the experiment. This practice does not lead to the potentially misleading assumption that the calculated buffer position is accurate, whereas H_2 may have leaked into the capsule during the experiment, thereby increasing the actual f_{H_2} value in the capsule. H_2 leakage may develop especially when a large f_{H_2} difference exists between the buffer system and the external pressure medium.

To circumvent this potential problem, we relied on the fact that at fixed P and T, the equilibrium assemblage annite + sanidine + magnetite + vapor defines the annite composition and f_{H_2} value. Therefore, the assemblage of annite + sanidine + magnetite + H_2O was run together with an f_{H_2} sensor to monitor the equilibrium f_{H_2} value generated by the system.

The low-temperature quench log $M_{Cl^-\,(25\ °C,\ 1\ bar)}$ values are converted to log f_{O_2} in Table 3 and presented in Figure 3 in log f_{H_2}. Experiment 11 used an initial sample of annite synthesized in sealed gold tubes without a surrounding buffer with the f_{H_2} condition set by the pressure vessel, slightly lower than NNO. To test whether this was an accurate equilibrium point, experiments 13 and 14 used annite containing different initial X_{Fe} compositions. Initial X_{Fe} values for experiments 13 and 14 annealed at the NNO and CCO buffers are 0.74 and 0.85, respectively. Magnetite was separated from the experimental products, and the X_{Fe} of the annite was measured by Mössbauer spectroscopy. Final X_{Fe} values for annite in experiments 13 and 14 are 0.69 and 0.72, respectively, indicating reproducible X_{Fe}. These data demonstrate significant compositional movement of the annite at relatively low temperatures. The possibility exists, however, that the equilibrium point is at some lower log f_{H_2} value. Experiment 18 used a modified triple-capsule configuration, similar to that shown in Figure 2C, consisting of the full assemblage recovered from experiment 11 and an f_{H_2} sensor. An additional external gold capsule contained the MH buffer. If the measured f_{H_2}-sensor value falls to that of the MH calibration, implying that the Eugster and

TABLE 3. Computation of log f_{O_2} from f_{H_2}-sensor data

Expt.	T (°C)	log $K_d(HCl^0)_{P,T}$	log$(m^s_{Cl^-})_{1,25}$	log$(m^s_{Cl^-})_{P,T}$	log$(m^s_{HCl^0})_{P,T}$	log$(m^r_{Cl^-})_{1,25}$	log$(m^r_{Cl^-})_{P,T}$	log$(m^r_{HCl^0})_{P,T}$	log$(f_{O_2})^{NNO}$	log$(f^s_{O_2})$
11	456	−1.955	−0.656	−1.353	−0.750	−0.537	−1.289	−0.622	−24.681	−24.166
13	459	−2.004	−0.716	−1.408	−0.812	−0.537	−1.310	−0.617	−24.543	−23.764
14	458	−1.986	−0.642	−1.358	−0.731	−0.537	−1.302	−0.619	−24.589	−24.142
18	460	−2.004	−0.810	−1.461	−0.917	−0.537	−1.310	−0.617	−24.497	−23.296
38	470	−2.175	−0.611	−1.427	−0.679	−0.550	−1.394	−0.613	−24.044	−23.780
69	400	−1.070	−0.631	−0.978	−0.886	−0.420	−0.845	−0.619	−27.495	−26.426
70	400	−1.070	−0.668	−1.002	−0.933	−0.420	−0.845	−0.619	−27.495	−26.237

Note: Data generated from low-temperature experiments by using configuration "C" shown in Figure 2, and the full annite + sanidine + magnetite assemblage. $K_d(HCl^0)$ is dissociation constant for $HCl^0 = H^+ + Cl^-$; from Frantz and Marshall (1984) and using density data from Burnham et al. (1969). HCl^0 represents associated HCl. Log$(m^s_{Cl^-})_{P,T}$ = ½(log $K_d(HCl^0)_{P,T}$ + log$(m^s_{HCl^0})$); an analogous procedure is used if reference (r) values are sought. Log$(m^s_{HCl^0})_{P,T}$ computed from $(m_{HCl^0})_{P,T} = (m_{Cl^-})_{1,25°C} - (m_{Cl^-})_{P,T}$. Log$(m^r_{HCl^0})_{P,T}$ from Frantz and Popp (1979) and unpublished data (Cygan). Log$(f_{O_2})^{NNO}$ computed from Haas (in Chou 1987b). Log$(f^s_{O_2})$ computed from Equation 9; r = reference, s = sample.

Wones (1962) bracket is correct, then the Cl^- measurements from experiments 11, 13, and 14 may be related to some other adjustment in annite composition or perhaps grain-size effects. The quench M_{Cl^-} value for experiment 18 clearly approaches the results of our other experiments at this temperature, indicating the equilibrium redox condition for Reaction 1 at an intermediate point between the MH and NNO buffers. This datum (shown in Fig. 3) provides a minimum value for the equilibrium constant (Eq. 2) at 460 °C.

Additional experiments at 400 °C used configurations similar to those at 460 °C; however, the annite compositions were not measured. H_2 sensors for these low temperatures were constructed from platinum tubing with a wall thickness of 0.1 mm to help facilitate H_2 permeation through the sensor walls. Past work has demonstrated that H_2 permeation is not hindered at T as low as 300 °C (Chou and Cygan unpublished data). Our results are given in Figure 3. Durations for experiments 69 and 70 are 432 and 792 h, respectively. Although this is an unreversed point, the consistency in log $M_{Cl^-(25\,°C,\,1\,bar)}$ values of the f_{H_2} sensor suggests that equilibrium was achieved. This assertion is further supported when viewed against duplicate experiment 70 with a doubled experimental duration.

As in the more reducing experiments previously discussed, the low-temperature, more oxidizing data similarly exhibit a divergence from previous studies but to higher log f_{H_2} conditions. Results indicate a decrease in temperature of the annite stability field at any given log f_{H_2}. This result is consistent with the results of our high-temperature data and our premises that f_{H_2} conditions in the vicinity of NNO of previous studies were accurately buffered, and that the equilibrium curve rotates around the data obtained under moderate f_{H_2} buffers such as NNO. The equilibrium constant of Equation 1 at 2 kbar can therefore be represented by the following relation (valid between 400 and 840 °C):

$$\log f_{H_2}(\pm 0.08) = 13.644 - \frac{17368}{T,\,K} + \frac{5.168 \times 10^6}{(T,\,K)^2}. \qquad (9)$$

Because low-temperature experiments are less well constrained, we suggest caution in applying the results of these experiments to low temperatures.

DISCUSSION

Results of selected experiments and past studies have been converted, where necessary, to f_{O_2} values to illustrate the change in the annite stability field with respect to buffer assemblages at 2 kbar. The possibility of nonideal H_2-H_2O gaseous behavior is a concern in this system because of the large H_2 partial pressures developed by the more reducing buffers. Therefore, to assess our assumption of ideal mixing, we computed activity-composition relations using the FLUIDTAB computer program and a modified Redlich-Kwong equation of state for high T (Grevel and Chatterjee 1992). Fugacity coefficients for pure H_2 and H_2O are calculated from the RKMIX computer program (Holloway 1977). Experiment 57, which was run on the WO buffer at 822 °C and an f_{H_2} value of 119.7 bars, was used as an example. The log f_{H_2O} and log f_{O_2} values calculated with the mixing model are 3.193 and −15.63, respectively. Conversely, assuming unit activity of H_2O, the log f_{H_2O} and log f_{O_2} values are 3.206 and −15.60, respectively. These log f_{O_2} values are within the experimental uncertainty of our f_{H_2}-sensor measurements, and we therefore ignored these corrections in our calculations.

Previously unpublished, low-temperature calibration data on the NNO buffer and data from Frantz and Popp (1979) were used to convert f_{H_2}-sensor measurements to f_{O_2} values. The HCl dissociation constant, $K_d(HCl^0)$, is taken from Frantz and Marshall (1984). For comparison with previous studies, these values, together with reference-calibration log $M_{Cl^-(25\,°C,\,1\,bar)}$ values, were used to compute log $(f_{O_2})_{P,T}$ through the relation

$$\log(f^s_{O_2})_{P,T} = \log(f^r_{O_2})_{P,T} + 4[\log(m^r_{HCl^0}) - \log(m^s_{HCl^0})_{P,T}] \qquad (10)$$

where superscripts r and s denote the reference and sample, in this instance, NNO and the annite + sanidine + magnetite + H_2O assemblage, respectively. Results are given in Table 3 and shown in Figure 4. The most notable difference is the expansion of annite stability to higher

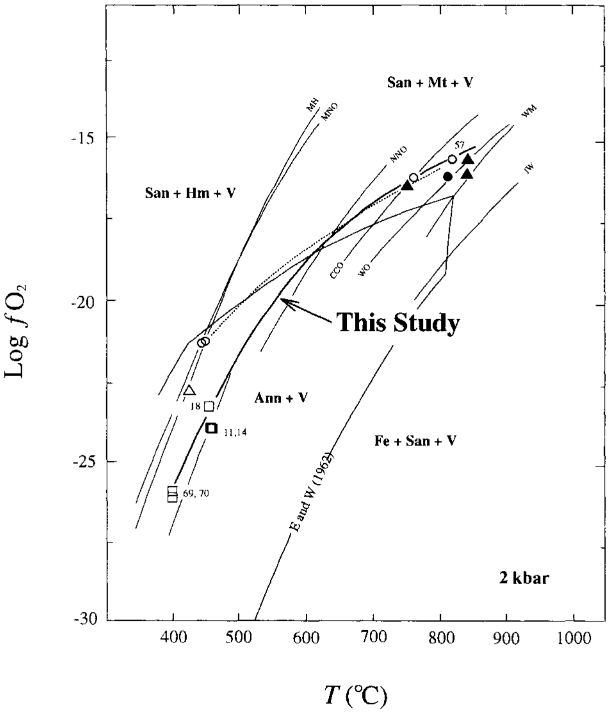

Figure 4. Annite stability field determined from the results of this study compared with that of other investigations in terms of log f_{H_2} vs. T (°C) at 2 kbar. The results of selected experiments from this study were used to determine the equilibrium curve for Reaction 1. Buffer curve abbreviations, as well as symbols, are as in Figures 1 and 3. One additional buffer is shown, the Fe + $Fe_{1-x}O$ + H_2O assemblage (IW) tabulated by Haas (in Chou 1987a). The annite + vapor (V) stability field from Eugster and Wones (1962) is shown as light solid lines; the light dotted curve is from Hewitt and Wones (1984). The heavy solid curve describes the results of this study.

f_{O_2} and temperature conditions. The fayalite + leucite + magnetite field is not yet intersected (Eq. 8) at the maximum temperature investigated. Similarly, the annite stability field changes at the lowest temperatures studied. At T = 400 °C, the annite + vapor field does not extend to MH buffer conditions as indicated by Eugster and Wones (1962). In general, the isobaric univariant curve of Reaction 1 is more subparallel to the trend of the buffer curves than in past studies.

We used the computer routine SUPCRT92 (Johnson et al. 1991) to compute the equilibrium curve for Equation 1. This curve is shown as a thick solid line in Figure 5. The SUPCRT92 database uses experimental data on the ASM reaction from Wones et al. (1971) to extract a $\Delta_f H^{\text{annite}}_{1,\,298.15}$ value (standard-state in SUPCRT92 is unit activity for the pure component at P and T). For comparison we also show the results of this study as a light solid line and the end-member annite curve of Hewitt and Wones (1984) as a light dot-dash line. Note the steeper slope of the curve of Hewitt and Wones (1984) relative to the results of this study, indicating the influence of lower T in their experiments.

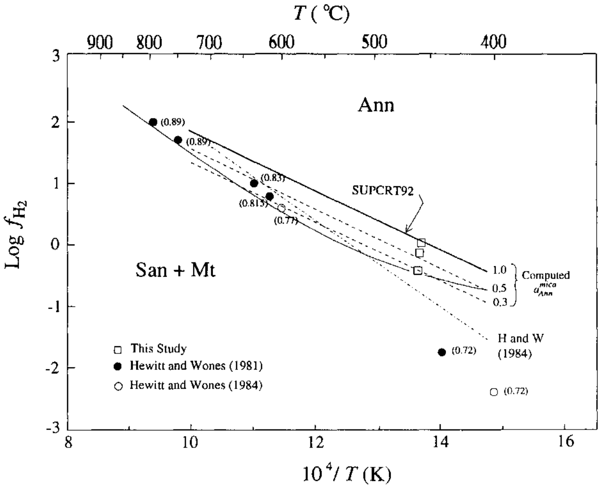

Figure 5. Log f_{H_2} vs. $10^4/T$ (K) diagram as in Figure 3 showing data on the annite–oxy-annite binary as solid and open circles from Hewitt and Wones, 1981 and 1984, respectively, and those of this study as open squares. Results of this study are depicted as a light solid line. The $a^{\text{mica}}_{\text{annite}}$ values, defined as the Fe^{2+} mole fraction, are given in parentheses alongside. The heavy solid line represents the equilibrium curve for the boundary between pure annite and sanidine + magnetite calculated using the computer routine SUPCRT92 (Johnson et al. 1991). The two dashed lines represent contour lines of equal activity (a = 0.5 and 0.3) of annite in the mica. The light dot-dash curve, labeled "H and W (1984)", shows the a = 1 position determined from the Hewitt and Wones (1984) assessment of annite stability.

Equation 2 can be used to calculate the activity of annite at various mole fractions of oxy-annite, assuming $a = X_{\text{Fe}}$. The standard state for annite is defined as the pure end-member annite at pressure and temperature, and, from Equation 2, $K_1 = f_{H_2}/a_{\text{annite}} = f^*_{H_2}$, where $f^*_{H_2}$ is the f_{H_2} in equilibrium with end-member annite at T. Therefore,

$$\log K_1 = (\log f_{H_2} - \log a_{\text{annite}}) = \log f^*_{H_2}. \qquad (11)$$

These results are shown in Figure 5 as dashed lines labeled with $a^{\text{mica}}_{\text{annite}}$ values of 0.5 and 0.3. Data points from past studies representing measurements of X_{Fe} in the annite–oxy-annite binary (Hewitt and Wones 1981, 1984) are also shown, along with the corresponding X_{Fe} values in parentheses (for this diagram, the mole fraction of Fe^{2+} in the mica). These binary data should locate near the intersection of the appropriate $a^{\text{mica}}_{\text{annite}}$ curves and the results of this study. The values are in reasonable agreement with those predicted by the activity contour lines at high temperature. However, they diverge with decreasing T and increasing Fe^{3+}. As the mole fraction of Fe^{3+} (the oxy-annite component) increases at lower T, the degree of nonideal mixing should likewise increase. Additionally, the data points at 440 and 400 °C lie significantly lower than our results and should likely be translated to higher log f_{H_2} values, given our contention of H_2 leakage into the capsule at these oxidizing conditions. These data suggest, of course, that the assumption of ideal mixing in the mica over this T range is a poor one and that activity coefficients, an alternative mixing model, or both are required. This aspect of annite–oxy-annite systematics, however, is beyond the scope of this study.

A recent study of Equation 1 by Dachs (1994) and a related one using Mössbauer spectroscopy to characterize synthetic annite compositions (Redhammer et al. 1993) both used hydrothermal techniques combined with f_{H_2} sensors to define the equilibrium and conditions of annite synthesis. Their data suggest a markedly different annite stability field at $T < 700$ °C relative to this study and that of Hewitt and Wones (1984). These differences probably result from H_2 leakage in the experiments of Dachs (1994) and Redhammer et al. (1993) owing to their use of H_2O mixed with oil as the pressure medium [Chou and Cygan (1990); Chou (submitted)].

The problem of H_2 containment in capsule configurations at both oxidizing and moderately reducing conditions has been discussed extensively (cf. Chou 1987a; Chou and Cygan 1990). Hydrothermal experimentation made at highly reduced conditions, such as f_{H_2} conditions associated with the buffer assemblage wüstite + magnetite + H_2O (WM) or iron + wüstite + H_2O (IW), require careful monitoring of the redox state actually produced at P and T by these buffers (Cygan and Chou 1994). Data from Haas (in Chou 1987a) were used to draw the curves, shown in Figure 4, of the predicted f_{O_2} values for these additional buffers. Preliminary f_{H_2}-sensor data using the capsule configuration shown in Figure 2C and 0.3 mm thick gold-wall capsules at 2 kbar, between 650 and 800 °C, and on the WM assemblage indicate that significant H_2 leakage occurred. The leakage was exacerbated when H_2O was used as the pressure medium. Therefore, the reaction

$$\text{annite} + 3\,H_2 = \text{sanidine} + 3\,\text{iron} + 4\,H_2O \quad (12)$$

warrants particular attention because the methodology used to determine this equilibrium point at high T is subject to uncertainties similar to those already discussed and because the probability of H_2 leakage is high. If leakage out of the capsule occurs, the previously reported equilibrium location for Equation 12 along a buffer curve at a given T may actually be located at less reduced conditions. These same arguments could be made in other hydrothermal studies under very reduced conditions unless buffering accuracy is determined. As noted above, improvements in experimental apparatus and buffering capabilities should allow accurate redox control. Of particular interest in this respect is the internally heated pressure vessel with modified capsule chambers (Scaillet et al. 1992). This apparatus uses modified AgPd membrane designs coupled with an internal gold cell enabling improved f_{H_2} containment in the vessel at the hot spot. Another innovation is the development of the sliding sensor, which uses binary metal systems to exhibit solid-solution behavior (Taylor et al. 1992). These developments and improvements in experimental apparatus and techniques hold promise in extending the range of high f_{H_2} values that are reliably generated, as well as buffer duration and its accurate measurement.

ACKNOWLEDGMENTS

This manuscript benefitted from the diligent reviews provided by B. Seal, H.T. Haselton, R. Popp, and D. Hewitt. We had many helpful discussions with our colleagues at the U.S. Geological Survey and elsewhere, in particular R. Berman and P. Candela. We are grateful to J.S. Huebner, J.J. Hemley, and H.T. Haselton for use of their laboratories and equipment.

REFERENCES CITED

Appleman, D.E., and Evans, H.T., Jr. (1973) Job 9214: Indexing and least-squares refinement of powder diffraction data. U.S. Geological Survey, Computer Contribution 20, U.S. National Technical Information Service, Document PB2-16188.

Burnham, C.W., Holloway, J.R., and Davis, N.F. (1969) Thermodynamic properties of water to 1,000 °C and 10,000 bars. Geological Society of America Special Paper 132, 96 p.

Chou, I-M. (1978) Calibration of oxygen buffers at elevated P and T using the hydrogen fugacity sensor. American Mineralogist, 63, 690–703.

——— (1986) Permeability of precious metals to hydrogen at 2 kb total pressure and elevated temperatures. American Journal of Science, 286, 638–658.

——— (1987a) Oxygen buffer and hydrogen sensor techniques at elevated pressures and temperatures. In G.C. Ulmer and H.L Barnes, Eds., Hydrothermal experimental techniques, p. 61–99. Wiley, New York.

——— (1987b) Calibration of the graphite-methane buffer using the f_{H_2} sensors at 2-kbar pressure. American Mineralogist, 72, 76–81.

Chou, I-M., and Eugster, H.P. (1976) A sensor for hydrogen fugacities at elevated P and T and applications. Eos, 57, 340.

Chou, I-M., and Cygan, G.L. (1990) Quantitative redox control and measurement in hydrothermal experiments. In R.J. Spencer and I-M. Chou, Eds., Fluid mineral interactions: A tribute to H.P. Eugster, p. 1–15. Geochemical Society Special Publication no. 2, University Park, Pennsylvania.

Cygan, G.L., and Chou, I-M. (1990) The assemblage $WO_2 + H_2O$ as a steady-state hydrogen source in moderately reduced hydrothermal experiments. American Mineralogist, 75, 1399–1405.

Cygan, G.L., Chou, I-M., and Sherman, D.M. (1991) Reassessment of the annite breakdown reaction using new hydrothermal experimental techniques. Eos, 72, 313.

Cygan, G.L., and Chou, I-M. (1994) An examination of the wüstite-magnetite-H_2O buffer at 2 kbars using f_{H_2}-sensors. Eos, 75, 137.

Dachs, E. (1994) Annite stability revised: 1. Hydrogen-sensor data for the reaction annite = sanidine + magnetite + H_2. Contributions to Mineralogy and Petrology, 117, 229–240.

Eugster, H.P. (1957) Heterogeneous reactions involving oxidation and reduction at high pressures and temperatures. Journal of Chemical Physics, 26, 1760–1761.

——— (1959) Reduction and oxidation in metamorphism. In P.H. Abelson, Ed., Researches in geochemistry, p. 397–426. Wiley, New York.

Eugster, H.P., and Wones, D.R. (1962) Stability relations of the ferruginous biotite, annite. Journal of Petrology, 3, 82–125.

Eugster, H.P., and Skippen, G.B. (1967) Igneous and metamorphic reactions involving gas equilibria. In P.H. Abelson, Ed., Researches in geochemistry, vol. II, p. 492–520. Wiley, New York.

Ferrow, E.A. (1990) The relation between c dimension and exchange components in micas. Mineralogy and Petrology, 43, 23–35.

Frantz, J.D., and Popp, R.K. (1979) Mineral-solution equilibria: I. An experimental study of complexing and thermodynamic properties of aqueous $MgCl_2$ in the system MgO-SiO_2-H_2O-HCl. Geochimica et Cosmochimica Acta, 43, 1223–1239.

Frantz, J.D., and Marshall, W.L. (1984) Electrical conductances and ionization constants of acids and bases in supercritical aqueous fluids: I Hydrochloric acid from 100 to 700°C and at pressures to 4000 bars. American Journal of Science, 284, 651–667.

Grevel, K.D., and Chatterjee, N.D. (1992) A modified Redlich-Kwong equation of state for H_2-H_2O fluid mixtures at high pressures and at temperatures above 400°C. European Journal of Mineralogy, 4, 1303–1310.

Hewitt, D.A. (1978) A redetermination of the fayalite-magnetite-quartz equilibrium between 650°C and 850°C. American Journal of Science, 278, 715–724.

Hewitt, D.A., and Wones, D.R. (1981) The annite-sanidine-magnetite equilibrium. GAC-MAC Joint Annual Meeting, Calgary, A-66.

——— (1984) Experimental phase relations of the micas. In Mineralogical Society of America Reviews in Mineralogy, 13, 201–256.

Holloway, J.R. (1977) Fugacity and activity of molecular species in supercritical fluids. In D.G. Frasier, Ed., Thermodynamics in geology, p. 166–181. Reidel, Boston.

Huebner, J.S., and Sato, M. (1970) The oxygen fugacity-temperature relationships of manganese oxide and nickel oxide buffers. American Mineralogist, 55, 934–952.

Johnson, J.W., Oelkers, E.H., and Helgeson, H.C. (1991) SUPCRT 92: A software package for calculating the standard molal thermodynamic properties of minerals, gases, aqueous species, and reactions from 1 to 5000 bars and 0° to 1000°C. Computers and Geosciences, 18, 899–947.

Partin, E., Hewitt, D.A., and Wones, D.R. (1983) Quantification of ferric iron in biotite. Geological Society of America Annual Meeting, 659.

Rebbert, C.R., and Hewitt, D.A. (1986) Biotite oxidation in hydrothermal systems: An experimental study. International Mineralogical Association, 207.

Redhammer, G.J., Beran, A., Dachs, E., and Amthauer, G. (1993) A Mössbauer and X-ray diffraction study of annites synthesized at different oxygen fugacities and crystal chemical implications. Physics and Chemistry of Minerals, 20, 382–394.

Robie, R.A., Hemingway, B., and Fisher, J.R. (1979) Thermodynamic properties of minerals and related substances at 298.15 K and 1 bar (10^5 Pascals) pressure and at higher temperatures. U.S. Geological Survey Bulletin 1452 (reprinted with corrections).

Rutherford, M.J. (1969) An experimental determination of iron biotite-alkali feldspar equilibria. Journal of Petrology, 10, 381–408.

Scaillet, B., Pichavant, M., Roux, J., Humbert, G., and Lefèvre, A. (1992) Improvements of the Shaw membrane technique for measurement and control of f_{H_2} at high temperatures and pressures. American Mineralogist, 77, 647–655.

Taylor, J.R., Wall, V.J., and Pownceby, M.I. (1992) The calibration and application of accurate redox sensors. American Mineralogist, 77, 284–295.

Wones, D.R. (1981) Mafic silicates as indicators of intensive variables in granitic magmas. Mining Geology, 31, 191–212.

Wones, D.R., and Eugster, H.P. (1965) Stability of biotite: Experiment, theory and application. American Mineralogist, 50, 1228–1272.

Wones, D.R., and Gilbert, M.C. (1969) The fayalite-magnetite-quartz assemblage between 600 and 800°C. American Journal of Science, 267, 480–488.

Wones, D.R., Burns, R.G., and Carroll, B.M. (1971) Stability and properties of synthetic annite. Eos, 52, 369.

Ziegenbein D., and Johannes, W. (1980) Graphite in C-H-O fluids: An unsuitable compound to buffer fluid composition at temperatures up to 700°C. Neues Jahrbuch für Mineralogie Monatshefte, 19, 289–305.

MANUSCRIPT RECEIVED AUGUST 22, 1994
MANUSCRIPT ACCEPTED NOVEMBER 13, 1995